

Multiferroic Properties of Pure, Transition-Metal and Rare-Earth–Doped BaFe₁₂O₁₉ Nanoparticles

Iliana N. Apostolova, Angel T. Apostolov, Steffen Trimper,* and Julia M. Wesselinowa

Different properties of pure and Ni, Zr, and Sm-doped BaFe₁₂O₁₉—bulk and nanoparticles—are investigated using a microscopic model and the Green's function technique. The magnetization M_s increases whereas the coercive field H_c decreases with increasing particle size. The doping leads to a decrease of M_s and the bandgap energy E_g with increasing Zr concentration x due to tensile strain and to an increase of M_s and E_g after Ni doping due to compressive strain as well as due to size effects. The behavior of the spontaneous polarization P_s and the real part ϵ' of the dielectric constant is opposite. The ϵ' of a pure BaFe₁₂O₁₉ nanoparticle decreases with increasing magnetic field h . The effects of Sm substitution at Ba or Fe sites on ϵ' and M_s are also studied.

1. Introduction


M-type barium hexaferrites BaFe₁₂O₁₉ (BFO) are materials with a large magnetization and magnetocrystalline anisotropy, high coercivity, and quite high Curie temperature $T_c^{\text{fm}} = 723$ K, allowing potential applications in various fields.^[1–3] The magnetic properties of pure BFO have been studied by many authors.^[4–9] The size dependence of the magnetization has been reported in previous studies.^[7,10,11]

Dr. I. N. Apostolova
Faculty of Forest Industry
University of Forestry
1756 Sofia, Bulgaria

Prof. A. T. Apostolov
Department of Physics
University of Architecture, Civil Engineering and Geodesy
1046 Sofia, Bulgaria

Prof. S. Trimper
Institute of Physics
Martin-Luther-University
Von-Seckendorff-Platz 1, 06120 Halle, Germany
E-mail: steffen.trimper@physik.uni-halle.de

Prof. J. M. Wesselinowa
Department of Physics
University of Sofia
Bldvd. J. Bouchier 5, 1164 Sofia, Bulgaria

 The ORCID identification number(s) for the author(s) of this article can be found under <https://doi.org/10.1002/pssb.202100069>.

© 2021 The Authors. physica status solidi (b) basic solid state physics published by Wiley-VCH GmbH. This is an open access article under the terms of the Creative Commons Attribution License, which permits use, distribution and reproduction in any medium, provided the original work is properly cited.

DOI: 10.1002/pssb.202100069

There are two different ways to modulate the magnetic properties of barium ferrite, namely, by substitution at Fe³⁺ or/and Ba²⁺ sites. Doping of BFO nanoparticles (NPs) with different ions causes an increase or decrease of the spontaneous magnetization M_s and the coercive field H_c .^[12–17] For example, M_s decreases by doping with Al³⁺ and Zr⁴⁺ ions,^[12,14,18] whereas it increases by doping with Ni²⁺, Co²⁺, or Cu²⁺ ions.^[13,17,19] Until now, the reason for such a different behavior is not clarified theoretically. Instead of that, there are some discrepancies in the reported results. For example, a decrease

of the coercive field H_c with increasing Al³⁺ doping concentration is observed in some studies,^[12,16,20] whereas an increase^[15,18] or a maximum in H_c is argued in Chen et al.^[21] The same situation is concerned in the magnetization M_s of Co²⁺-doped BFO. Although Feng et al.^[22] and Tran et al.^[23] have reported an increase of the magnetization with increasing Co²⁺ concentration, Chavan et al.^[24] and Kumar et al.^[25] have claimed a decrease of M_s . In the same manner, ion-doping substitution at either the Ba site or Fe site can differently modify the magnetic and electric properties of BFO. The substitution of Co²⁺ and Mn³⁺ ions at the Fe site reveals a larger effect on the permittivity than that of Sr²⁺ and Ca²⁺ ions at Ba sites.

The analysis of rare earth (such as La, Sc, Dy, Sm, Ho)–doped BFO has been conducted with increasing significance over the past several years.^[26–33] The spontaneous magnetization M_s , for instance, decreases by doping with Se³⁺ ions,^[30] whereas otherwise it increases by doping with Dy³⁺, La³⁺, or Sm³⁺ ions, as argued elsewhere.^[26,31,32]

A feature of BFO is the occurrence of multiferroic properties observed in thin films at room temperatures by Kumar et al.^[34] Simultaneously one finds pronounced ferroelectricity and strong ferromagnetism in BFO ceramics, as reported by Tan et al.^[4,35] The authors suggest the distortion of the Fe oxygen octahedron within a lattice unit of its perovskite-like hexagonal structure as the origin of the polarization. Based on first-principles simulations, Wang and Xiang^[36] have argued that M-type hexaferrite AFe₁₂O₁₉ with A = Ca, Sr, Ba, Pb, etc. exhibits a frustrated anti-ferroelectricity associated with its trigonal bipyramidal Fe³⁺ sites. The compressive strain induced by Al³⁺ or Ga³⁺ ion doping at the Fe³⁺ site is able to stabilize the ferroelectric state of BFO. Another aspect is the enhancement of the ferroelectric transition temperature of BFO by Al³⁺ ion doping.^[12] According to Turchenko et al.^[37] the spontaneous polarization P_s in BFO substituted with In, Al, Ga, and Sc is due to the absence of an inversion center in the unit cell. The polarization P_s is

enhanced in case of increased In doping.^[38] A magnetoelectric coupling in Sc-doped BFO is reported by Gupta et al.,^[39] where the polarization P_s as well as the dielectric constant ϵ' is reduced when an applied magnetic field h is increased.

The dielectric properties of Zr-doped BFO NPs were studied by Deng et al.^[14] They found an increase of ϵ' with increasing Zr dopants due to the replacement of Fe^{3+} by Zr^{4+} , and of the Fe^{3+} ions by Fe^{2+} ions to keep charge neutrality. The dielectric properties of BFO for different doping ions such as Al, La, Ni, Ti, and Dy have been reported in several studies.^[12,15–17,40] The dielectric constant ϵ' is enhanced if the doping concentration of Bi^{4+} and Ti^{16} increases, whereas ϵ' decreases for doping with La, Ni, Al, and Mg.^[15,17,40,42] The reason for such a different behavior is an open problem. The size dependence of ϵ' in BFO is reported by Kumar et al.^[43] The bandgap of BFO NPs for different doping ions has been studied elsewhere.^[40,44,45]

In view of the complex behavior of BFO, the aim of this article is to study the magnetic and dielectric properties of pure, transition metal, and rare earth ion doped BFO NP using a unified microscopic model, including the different but relevant interactions between the constituents. To the best of our knowledge, such a microscopic model is still missing. The origin of the aforementioned quite different behavior such as increase or decrease of magnetization, the dielectric constant, and other observable quantities by doping of BFO NPs with different ions at Ba and Fe sites is discussed and clarified on a microscopic level. Due to the different ionic radii of the doping ions compared to those of the host, the interaction constants are modified in a significant manner. The Green's function method is the appropriate method to attack the complex underlying interactions of the material

2. The Model

As emphasized, BFO offers as a pure and as an ion-doped material multiferroic properties. Therefore, the microscopic model has to include a magnetic part denoted as H_{s-d} , a ferroelectric Hamiltonian H_f , and the magnetoelectric coupling represented by H_{mf} . The total Hamiltonian is

$$H = H_{s-d} + H_f + H_{mf} \quad (1)$$

where the different parts have to be specified in the following. The magnetic properties of BFO offering a low-bandgap semiconductor^[46,47] are determined by the $s-d$ model given by

$$H_{s-d} = H_m + H_{el} + H_{m-el} \quad (2)$$

Here, H_m is the Heisenberg model describing the magnetic properties of the localized Fe^{3+} ions

$$\begin{aligned} H_m = & -\frac{1}{2} \sum_{ij} (1-x) J_{ij}^{\text{Fe-Fe}} \mathbf{S}_i^{\text{Fe}} \cdot \mathbf{S}_j^{\text{Fe}} \\ & -\frac{1}{2} \sum_{ik} x(x') J_{i,k}^{\text{Fe-DI}} \mathbf{S}_i^{\text{Fe}} \cdot \mathbf{S}_k^{\text{DI}} \\ & - D \sum_i (S_i^{\text{Fe}})^2 - K_1 \sin^2 \theta \sum_i S_i^{\text{Fe}} - g\mu_B \mathbf{h} \cdot \sum_i \mathbf{S}_i^{\text{Fe}} \end{aligned} \quad (3)$$

where \mathbf{S}_i is the spin operator of the Fe^{3+} spin at lattice site i . The magnetic subsystem shows anisotropic properties characterized

by the single-site anisotropy D , the first anisotropy constant K_1 , and the angle θ between the magnetization and the easy axis. According to Wang et al.^[48] there appears in BFO a second anisotropy constant $K_2 \ll K_1$, which can be neglected. The exchange interactions between the Fe–Fe and Fe-doping ions are denoted as $J^{\text{Fe-Fe}}$ and $J^{\text{Fe-DI}}$ in Equation (2). The five independent Fe^{3+} ions are coupled via O^{2-} anions by superexchange interactions forming a ferromagnetic structure.^[49]

The Hamiltonian H_{el} in Equation (2) represents the conduction band electrons

$$H_{el} = \sum_{ij\sigma} t_{ij} c_{i\sigma}^+ c_{j\sigma} \quad (4)$$

where t_{ij} is the hopping integral and $c_{i\sigma}^+$ and $c_{i\sigma}$ are Fermi creation and annihilation operators.

The operator H_{m-el} couples the two subsystems characterized by Equation (3) and (4) by an intra-atomic exchange interaction I_i . The Hamiltonian H_{m-el} is the well-established $s-d(f)$ model proposed by Vonsovskij^[50] and Nagaev^[51] for ferromagnetic semiconductors, where I is the coupling constant between the conduction s electrons and the localized d or f electrons. The Hamiltonian reads

$$H_{m-el} = \sum_i (1-x) I_i \mathbf{S}_i \cdot \mathbf{s}_i \quad (5)$$

Here, x is the ion-doping concentration. The spin operators \mathbf{s}_i of the conduction electrons at site i can be expressed by Fermi operators $s_i^+ = c_{i+}^+ c_{i-}$, $s_i^- = (c_{i+}^+ c_{i+} - c_{i-}^+ c_{i-})/2$.

The origin of the polarization in BFO is due to the shift of Fe^{3+} off the center of the FeO_6 octahedron.^[4,35] The underlying mechanism is well described by an Ising model in a transverse field

$$H_f = -\Omega \sum_i B_i^x - \frac{1}{2} \sum_{ij} (1-x') J'_{ij} B_i^z B_j^z \quad (6)$$

The pseudo-spin operator B_i^z characterizes the two positions of the ferroelectric unit at the lattice point i . The interaction between adjacent lattice sites is taken to be ferroelectric, i.e., $J'_{ij} > 0$. The dynamics of the model is determined by the operator B^x and the transverse field Ω favoring tunnel processes between the ferroelectric units. Because the ordered phase is characterized by the two nonzero ferroelectric order parameters $\langle B^x \rangle \neq 0$ and $\langle B^z \rangle \neq 0$, it is convenient to analyze the ferroelectric subsystem H_f (Equation (6)) in a rotated frame. The rotation angle ϕ in the $x-z$ plane is chosen in a manner that $\langle B^{x'} \rangle = 0$ in the new coordinate system.

Following Gutierrez et al.,^[52] we propose a linear magnetoelectric coupling between the magnetic and ferroelectric order parameters. With the coupling strength g , the Hamiltonian reads

$$H_{mf} = -g \sum_{jkl} B_j^z \mathbf{S}_k \cdot \mathbf{S}_l \quad (7)$$

The magnetization M

$$M = \frac{1}{N} \sum_i [(S+0.5) \coth[(S+0.5)\beta E_{mi}] - 0.5 \coth(0.5\beta E_{mi})] \quad (8)$$

is determined by the elementary excitations realized in the microscopic system. In Equation (8) E_{mi} is the spin wave energy, which can be calculated using Green's function. For the magnetic subsystem, we consider

$$g_{ij} = \langle\langle S_i^+; S_j^- \rangle\rangle \quad (9)$$

In the same manner, we get the relative polarization P in the form

$$P = \frac{1}{2N} \sum_i \tanh \frac{E_{fi}}{2k_B T} \quad (10)$$

As well as in the magnetic subsystem the polarization is determined by the elementary excitation energy E_{fi} . This pseudo-spin wave energy is obtained from Green's function

$$G_{ij} = \langle\langle B_i^+; B_j^- \rangle\rangle \quad (11)$$

The dielectric function $\epsilon(E)$ is likewise related to Green's functions. Following Vaks^[53] $\epsilon(E)$ is deduced from the equation

$$\left[\left(\frac{\Lambda}{\epsilon(E)} - 1 \right)_{\alpha\beta} + \Lambda \frac{k_\alpha k_\beta}{k^2} \right] G^{\beta\gamma}(E) = \delta_{\alpha\gamma} \quad (12)$$

with $\Lambda = 4\pi Z^2/\nu$ and the electron charge Z and ν the volume. To determine the real part ϵ' and the imaginary part ϵ'' of the dielectric function ϵ , we have to evaluate the real and imaginary parts of the longitudinal anticommutator pseudo-spin Green's function

$$G_{ij}^{zz}(E) = \frac{2 \langle B_i^z B_j^z \rangle (E^2 - (E_{fi})^2 + 2iE\gamma^{11})}{(E + i\gamma^{33})(E^2 - (E_{fi})^2 + 2iE\gamma^{11}) - E(\epsilon^{13})^2} \quad (13)$$

Here, E_{fi} and γ^{11} are the transverse pseudo-spin-wave energy and its damping, whereas γ^{33} is the longitudinal damping.

3. Numerical Results and Discussion

The NP is defined by fixing the origin at a certain Fe ion in the center of the particle and including all other Fe ions within the particle in shells. The shells are numbered by $n = 0, \dots, N$, where $n = 0$ corresponds to the central ion and $n = N$ represents the surface shell of the system. The numerical evaluations are based on the following model parameters: $J^{\text{Fe-Fe}} = 500 \text{ K}$,^[54] $D = -2.88 \text{ K}$,^[55] $K_1 = 3.3 \times 10^6 \text{ erg cm}^{-3}$ at $T = 300 \text{ K}$,^[56-59] $K_{1\text{surface}} = 1.8 \times 10^6 \text{ erg cm}^{-3}$, $J^{\text{Fe-Ni}} = 81 \text{ K}$,^[60] $J^{\text{Fe-Sm}} = -16.6 \text{ K}$,^[61] $I = 0.5 \text{ eV}$; $J' = 135 \text{ K}$; $\Omega = 20 \text{ K}$, $g = 20 \text{ K}$, $T_C^{\text{fm}} = 723 \text{ K}$,^[2,54] $T_C^{\text{Fe}} = 39 \text{ K}$,^[12] and $S = 5/2$ for Fe^{3+} and $S = 1/2$ for the pseudo-spins.

Following the calculation scheme of Isalgue et al.^[54] performed in mean field approximation, we have calculated the magnetization of BFO as a function of the temperature and a magnetic field within Green's function theory. Our approach includes correlation functions, which are beyond the random phase approximation. Moreover, our evaluation includes the single-ion anisotropy D and the uniaxial magnetocrystalline anisotropy K_1 , which has not been considered in Isalgue et al.^[54] Let us

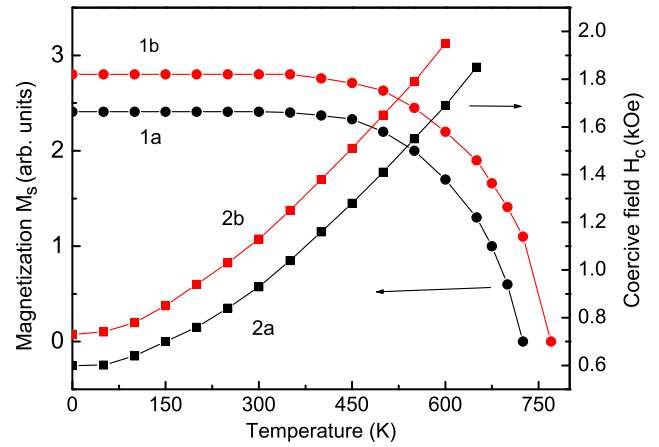


Figure 1. Temperature dependence of the spontaneous magnetization M_s (1) and of the coercive field H_c (2) for pure BFO for different anisotropic constants K_1 : (1a,2a) $3.3 \times 10^6 \text{ erg cm}^{-3}$; (1b,2b) $4.3 \times 10^6 \text{ erg cm}^{-3}$.

emphasize that the anisotropy is quite high in BFO, which gives rise to its large coercivity. The spontaneous magnetization M_s for pure BFO decreases with increasing temperature and vanishes at $T_C^{\text{fm}} = 725 \text{ K}$, which can be seen in **Figure 1**, curves 1a, 1b. The result is in agreement with the experimental data in previous studies.^[5,36] **Figure 1** offers also clear evidence for the influence of the magnetic anisotropy constant K_1 on the magnetization. The magnetization becomes larger for higher K_1 values (compare curve 1b); the Curie temperature T_C increases with increasing K_1 , too. This argument is also in agreement with the temperature-dependent spontaneous magnetization M_s of $\text{SrFe}_{12}\text{O}_{19}$ (SFO). The magnetocrystalline anisotropy constant K_1 of SFO is larger compared to that of BFO as observed in Shirk and Buessem.^[62] The authors found that K_1 for SFO is 10% higher than that of BFO over the whole temperature range. As a consequence, we should observe a larger magnetization in SFO compared to BFO; i.e., curve 1b in **Figure 1** could correspond to SFO. Indeed this result is in agreement with the experimental data for M_s in BFO and SFO reported by Shirk and Buessem.^[62] To clarify the role of the ion radii note that the radius of the Sr^{2+} ion (1.32 \AA) is smaller compared to that of Ba^{2+} (1.49 \AA). As a consequence, the Fe ions in SFO are closer together. Because the exchange interaction J is proportional to the inverse distance between the ions, the coupling J becomes larger in SFO compared to BFO. A larger J gives rise also to an enlarged magnetization in SFO. Moreover, the phase transition temperatures offer the relation $T_C(\text{SFO}) > T_C(\text{BFO})$. Since the transition temperature is proportional to J we conclude $J(\text{SFO}) > J(\text{BFO})$. The discussion reveals again that the magnetization of SFO is larger than that of BFO. The argument is also supported by a larger K_1 and the smaller Sr ion radius in comparison to Ba.

Let us further stress that the second case (see curve 1b in **Figure 1**) could be used to explain the increase of the spontaneous magnetization M_s in rare earth ion doped BFO (at the Fe sites). Namely, this increase of M_s in rare earth-doped BFO is clearly correlated to the large magnetocrystalline anisotropy and a large magnetostriction of the rare earth ions. The

magnetocrystalline anisotropy field increases with growing rare earth doping, for instance, with Ce^{3+} ^[63,64] and La^{3+} ion doping. Moreover, an increase of the rare earth dopant concentration x leads to a change of Fe^{3+} ions to Fe^{2+} ions, the magnetocrystalline anisotropy of which is higher than that of Fe^{3+} .

The temperature dependence of the coercive field H_c for different anisotropy values K_1 is also shown in Figure 1. H_c increases with increasing temperature T and anisotropy constant K_1 in accordance with the experimental data of previous studies.^[5,62] Regarding the discussion of the K_1 dependence of M_s , we obtain also a larger coercive field H_c value for SFO (curve 2b in Figure 1) in comparison to BFO (curve 2a in Figure 1) as reported in Shirk and Buessem.^[62]

Let us emphasize again that the exchange interaction $J_{ij} = J(r_i - r_j)$ depends on the distance between the interacting spins. Therefore, the coupling constants are influenced by the lattice parameters, the lattice symmetry, and the number of nearest neighbors. In particular, J_{ij} is proportional to the inverse of the distance between the two nearest spins. This observation has an important impact on the investigation of surfaces and ion-doping effects. Obviously, the exchange interactions at the surface J_s differs from those in the bulk J_b . Both effects $J_s > J_b$ and $J_s < J_b$ can be realized.

The size dependence of the spontaneous magnetization M_s and the coercive field H_c is shown in Figure 2 for $T = 300$ K and applying $J_s > J_b$. One realizes that M_s increases whereas H_c decreases with increasing NP size. The investigations suggest a critical size of around $N = 3$ shells, i.e., of 6 nm, where a ferromagnetic to superparamagnetic transition appears. The coercive field H_c decreases with increasing NP size due to multidomain formation and an easy movement of the domain walls. The theoretical finding is in good qualitative agreement with the experimental data presented in several studies.^[7,8,10,11,65] A very small increase of M_s and a strong one for H_c with increasing NP size was reported in Li et al.^[66] We should point out that there is a pronounced shape dependence of the magnetic properties of BFO nanoparticles as proposed in Kumar and Bhatnagar.^[67] The shape anisotropy has a significant value compared to other anisotropies. The discussion of the

shape of the NP and its influence on the magnetic order will be discussed in a forthcoming work.

Obviously the energy associated with the depolarization field should be more relevant in the nanomaterial^[68] than in the bulk. As already argued in Glinchuk and Morozovskaya,^[69] based on a phenomenological theory the effects of surface tension and a depolarization field are able to modify the phase diagrams of ferroelectric nanoparticles. Recently,^[68] the depolarization effects were discussed in the frame of microscopic models comparable to our approach. similar to the present one. Here we follow the line given in Tjablikov^[70] where the Hamiltonian for the ferroelectric part in Equation (1) is supplemented by a term

$$H_{\text{ed}} = \frac{1}{2} \sum_{ij} \Phi'_{ij} B_i^z B_j^z \quad (14)$$

The symmetric tensor Φ'_{ij} depends on the shape, the size, and the orientation of the particles. In case of spherical nanoparticles, the tensor is diagonal. The form of H_{ed} is suggested by the fact that depolarization effects are originated by the same interaction mechanism as the ferroelectricity itself. It is also in accordance with the phenomenological form of the underlying Gibbs free energy. Combining H_f and H_{ed} , it results that the depolarization field gives rise to altered effective couplings in Equation (6), i.e.

$$J'_{ij}{}^{\text{eff}} = J'_{ij} - \Phi'_{ij} \quad (15)$$

Because the coupling becomes smaller, the polarization is reduced in comparison to the bulk material. In the same manner the magnetic exchange interactions in Equation (3) become renormalized. The enhancement of the magnetization due to FE-ion doping is slightly weakened due to demagnetization fields. Therefore, the magnetization curve 1 in Figure 2 would be slightly reduced, too. The qualitative behavior of the polarization and magnetization due to ion doping remains unchanged. For a more quantitative understanding, we refer the reader to a forthcoming study.

In contrast, Tan et al.^[4] have reported the opposite behavior of the saturated polarization, i.e., P_s of BFO is strongly reduced with the increase of the grain size. In our model the polarization is calculated from Equation (10), where the excitation energy E_{fi} is determined by the exchange constants at the surface or in bulk as indicated in Equation (6). The mentioned behavior is observed in our model if the relation $J'_s < J'_b$ is fulfilled.

Another aspect is the influence of nonmagnetic ions. Here we have analyzed the effect of nonmagnetic Zr^{4+} ion doping on the magnetization M_s for the case $J_s = 1.5J_b$, which is valid for all used model parameters. The Zr^{4+} ions prefer to occupy the tetrahedral sites of the BFO lattice. The radius of the Zr^{4+} ion is assumed to be 0.72 Å. The value is larger compared to that of Fe^{3+} with 0.67 Å. Hence, the doping ion causes a tensile strain leading to an expansion of the crystal lattice with growing Zr content. As a consequence the exchange interaction parameter J_d in the doped states is reduced, i.e., $J_d < J_b$. A similar tensile strain, i.e., an enhancement of the lattice parameters with increasing Zr concentration x , was reported in previous studies.^[14,71] The concentration dependence of the spontaneous magnetization $M_s(x)$ is displayed in Figure 3. One sees a clear decrease of M_s with increasing Zr concentration x . The effect occurs due to the

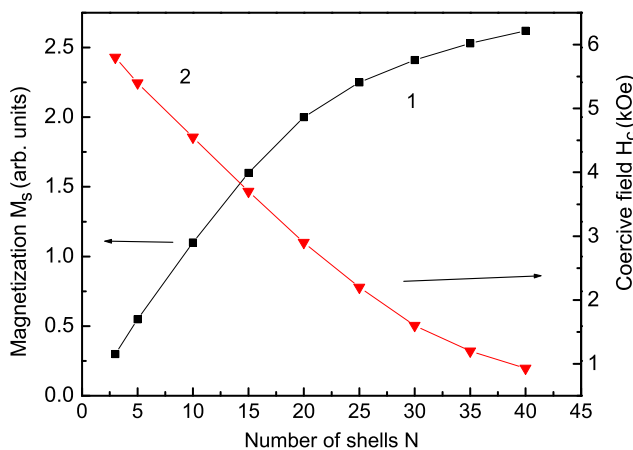


Figure 2. Size dependence of the spontaneous magnetization M_s (1) and of the coercive field H_c (2) of pure BFO for $K_1 = 3.3 \times 10^6$ erg cm^{-3} , distance between the shells is 2 nm, $J_s = 1.5J_b$, and $T = 300$ K.

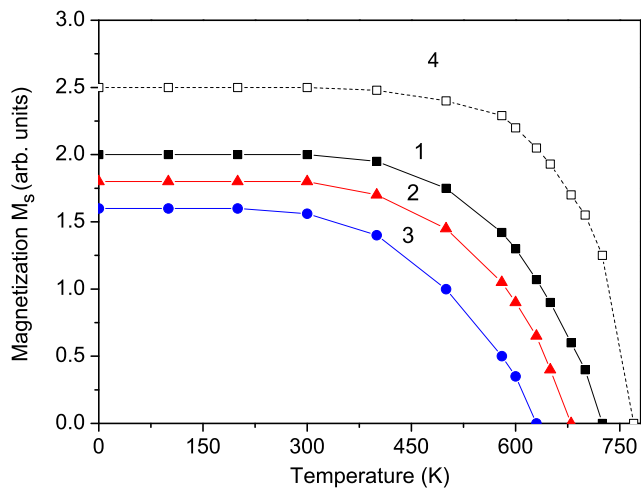


Figure 3. Temperature dependence of the spontaneous magnetization M_s of a BFO NP ($N = 20$ shells) for different Zr doping concentrations x , $J_d = 0.6J_b$, (1) $x = 0$; (2) $x = 0.1$; (3) $x = 0.3$; and (4) for Ni doping concentration with $x = 0.3$, $J_d = 1.2J_b$.

substitution of Fe^{3+} ions by nonmagnetic Zr^{4+} ions. The reduction of the spontaneous magnetization M_s is in agreement with the experimental data offered in the previous studies.^[14,72] Simultaneously, the Curie temperature T_C decreases with increasing x . An increasing Zr concentration x is attended by a conversion of Fe^{3+} ions (high spin) into Fe^{2+} (low spin). The substitution of Fe^{3+} by Zr^{4+} ions guarantees the charge neutrality. Moreover, these dopants lead to a weakening of the superexchange interactions between the Fe^{3+} and O^{2-} ions, which may also cause the reduction of the spontaneous magnetization M_s . Accordingly the magnetic phase transition temperature T_C^{fm} decreases if the Zr content x is increased. In the same manner, one observes a decrease of M_s of BFO with increasing Co dopants. The Co^{2+} ions reveal an ionic radius of 0.82 \AA , which is also larger than that of the Fe^{3+} ions with 0.64 \AA . The result is in agreement with the experimental data in previous studies,^[24,25] but in contrast to other studies.^[22,23] Note that the magnetocrystalline anisotropy K_1 increases with increasing ion doping for example by $\text{Zn}^{[73]}$ or $\text{Ru}^{[74]}$ ions. The enhanced anisotropy and the simultaneous reduction of the particle size are useful for many applications, such as improving of the signal noise ratio and the stability of recording devices.

Our model is able to explain also the decrease of the spontaneous magnetization M_s by doping with different ions, for example, Nd, La, Sm, Sc, Ti, Ga, Dy, In, and Zn ions^[8,16,31,75–82] where the radius of these ions is larger compared to that of Fe. For example, the radii of the rare earth Sc and Sm ions are $r = 0.89 \text{ \AA}$ and $r = 0.96 \text{ \AA}$, respectively, and consequently larger than that of Fe ions with $r = 0.67 \text{ \AA}$. The observed tensile strain gives rise to $J_d < J_b$ and to a decrease of the magnetization with increasing Sc or Sm dopant concentration. For completeness, let us mention that Baykal et al.^[83] have obtained contrary to our result and to that of Tanwar et al.^[81] an increase of the magnetic moment by substitution of nonmagnetic Zn^{2+} ions at the Ba site in BFO.

Generally, doping with ions, the radius of which is smaller compared to other ions, there appears a compressive strain.

As a consequence, the exchange interaction constant in the doped state is larger compared to that in the undoped case, i.e., $J_d > J_b$. Such a situation is realized by doping with Cu or Ni ions. The radii of those ions are smaller compared to the Fe ion. So the exchange parameters of Cu- or Ni-doped material are larger than the undoped case, which leads to an increase of the spontaneous magnetization M_s with increasing ion-doping concentration x . The situation is shown in Figure 3, curve 4. The result of our theoretical approach is in agreement with experimental findings in Vadivelan and Jaya^[19] where Cu ion is the dopant, or Ni ion doping in previous studies.^[17,84,85]

As already mentioned before, a simultaneous occurrence of large ferroelectricity and strong ferromagnetism has been observed in barium and lead hexaferrite ceramics.^[4,35] The FeO_6 octahedron in its perovskite-like hexagonal unit cell and the shift of Fe^{3+} off the center of the octahedron are suggested to be the origin of the polarization in BFO.^[4] Now we present the temperature dependence of the spontaneous polarization P_s shown in Figure 4, curve 1. Note that we have obtained a clear ferroelectric hysteresis loop, which is not shown here. In the following we analyze the Zr ion doping dependence of P_s . As the result of Zr doping the spontaneous polarization P_s and the critical temperature T_C^{Fe} in BFO increase with increasing concentration x ; see Figure 4, curves 2,3. Let us remark that the mechanism for the occurrence of a polarization in ferrite is similar to the conduction process mentioned before. The occupation of the tetrahedral sites by Zr^{4+} ions tends to force some of the Fe^{3+} ions to migrate from tetrahedral to octahedral sites. The raised number of Fe^{3+} ions at octahedral sites enhances consequently the electronic hopping between Fe^{2+} and Fe^{3+} sites. Unfortunately, experimental data for the spontaneous polarization P_s in Zr-doped BFO are still missing. Otherwise an increase of P_s with increasing doping concentration in In- and Al-doped BFO was observed by Trukhanov et al.^[80] In addition, the influence of Ni ion doping on the spontaneous polarization P_s is shown in Figure 4, curve 4. The polarization decreases with increasing doping concentration x .

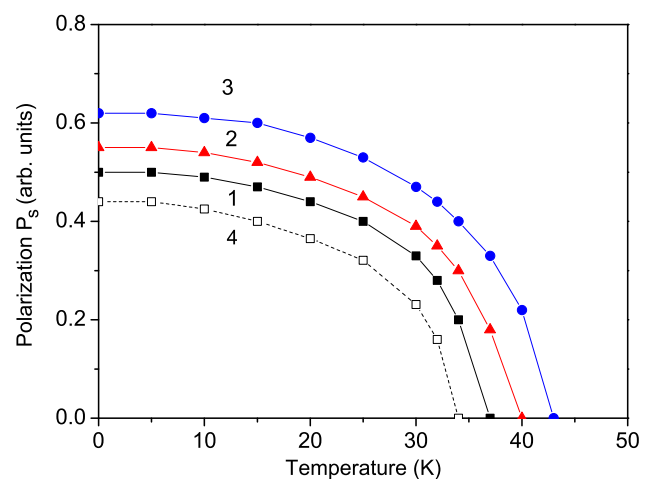


Figure 4. Temperature dependence of the spontaneous polarization P_s of a BFO NP ($N = 20$ shells) for different Zr doping concentrations x ; $J'_d = 1.2J'_b$: (1) $x = 0$; (2) $x = 0.1$; (3) $x = 0.3$; (4) Ni doping concentration $x = 0.2$, $J'_d = 0.9J'_b$.

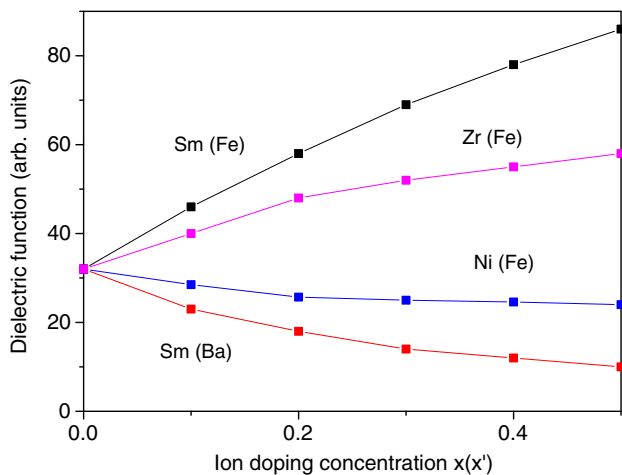


Figure 5. Doping concentration dependence of the dielectric function ϵ' of a Zr (Fe), Ni(Fe), Sm(Fe), and Sm (Ba) doped BFO NP with $N = 20$ shells and for $T = 300$ K. x stands for concentration of Zr, Ni, Sm doping at Fe site, x' for Sm doping at Ba site.

The doping dependence of the dielectric function ϵ' is also calculated and the results are presented in **Figure 5**. The dielectric function ϵ' grows with increasing Zr doping concentration. Such an increase of ϵ' is connected with the above mentioned migration process where some of the iron ions migrate from tetrahedral to octahedral sites due to the occupation by Zr^{4+} .^[86] Experimental investigations indicate a similar behavior, namely an increasing of the dielectric constant ϵ' with increasing x as it has been reported in refs. [16,43,87,88] for In and Ti doped BFO.

Let us point out that our model provides an explanation for the doping dependence of the dielectric function ϵ' with ions causing compressive strain opposite to the Zn doping giving rise to a tensile strain. To illustrate this fact, we have analyzed doping with Ni^{2+} ions, the radius of which is smaller than that of Fe^{3+} ; the lattice parameters decrease after Ni ion doping.^[40] The result is shown in **Figure 5** where ϵ' decreases with increasing Ni doping concentration x . Here our results are in good agreement with the experimental data of Sharma et al.^[40] and Dawar et al.^[17] but in disagreement with the results reported in Waqar et al.^[85] which offered an increase of ϵ' with increasing Ni concentration.

It should be pointed out that due to continued doping on Fe or Ba sites the solid solution limit can be achieved and consequently a second phase will be established. The reported experimental data by Sm (Fe) ion doping of Luo et al.^[91] and by Sm (Ba) of Wang et al.^[32] are for $x = 0-0.3$ and $x = 0-0.5$, respectively, by Ni (Fe) ion doping of Waqar et al.^[85] for $x = 0-0.5$, and by Zr (Fe) doping of Liu et al.^[16] for $x = 0-0.5$. This finding is included in **Figure 5**.

Sharma et al.^[40] attributed the decrease of ϵ' with increase Ni to increase of the bandgap. To clarify the situation, we calculated the bandgap energy E_g for Ni-doped BFO NP from the equation

$$E_g = \omega^+(\mathbf{k} = 0) - \omega^-(\mathbf{k} = \mathbf{k}_\sigma) \quad (16)$$

This relation determines the difference between the valence and conduction band. Experimentally the bandgap is $E_g = 3.58$ eV for undoped bulk BFO.^[89] The corresponding value

$E_g = 2.98$ eV^[90] is larger than that in BFO thin films of thickness $d = 6.7$ nm. Other studies^[44] yield $E_g = 2.87$ eV for an NP with size of $d = 17.65$ nm, whereas in Parween^[92] a bandgap of $E_g \approx 2$ eV for an NP with average particle size of 49 nm has been reported. Bandgaps of $E_g = 1.86$ eV or $E_g = 1.82$ eV were observed in a pure BFO NP for the coprecipitation and ceramic method by Frias et al.^[46] **Figure 6**, curve 1, shows the Ni doping dependence of E_g in a BFO NP with $N = 20$ shells. The bandgap energy E_g increases with increasing Ni dopant concentration $x = 0 - 0.2$. The result is in agreement with the related experimental data in refs. [40,44]. The behavior $E_g(x)$ is obviously related to the strong $s-d$ exchange interaction. This is shown in **Figure 6**, curve 2, where an increase of the $s-d$ interaction constant I in Equation (5) leads to an increased value of E_g . Actually, the Coulomb interaction and an external magnetic field are likewise able to modify the band energies. The effects are not considered yet. In contrast to the previous case the bandgap E_g in a Zr-doped BFO NP is reduced with increasing Zr concentration, which is shown in **Figure 6**, curve 3. In that case, there appears a tensile strain due to an expansion of the lattice. Such a situation is already discussed for the magnetization in Zr-doped BFO. Note that the behavior of the bandgap energy E_g in the cases of Ni or Zr seems to be related, namely, by an inverse relationship between the crystallite size and the bandgap energy based on quantum confinement effects.^[44,93] Unfortunately, we are not aware of experimental data for bandgap values of Zr-doped BFO. However, Habanjar et al.^[45] have observed a similar decrease of E_g by adding Co ions to BFO, leading to tensile strain, too.

As already mentioned, there are two different ways to modulate the magnetic properties of barium ferrite, substitution at Fe^{3+} or at Ba^{2+} sites. Therefore, we have studied the effects of substituting Fe or Ba ions by rare earth Sm ions. The effect is closely connected with the ionic radii. For the Sm^{3+} ion the radius is 0.96 Å. The value is larger than that from the Fe^{3+} ion (0.67 Å), but smaller than that of the Ba^{2+} ion (1.49 Å). Accordingly, it results in a tensile strain in the first case, leading to $J_d < J_b$, $J'_d > J'_b$,^[30,39] whereas in the second one, the lattice parameters decrease, i.e., a compressive strain appears with

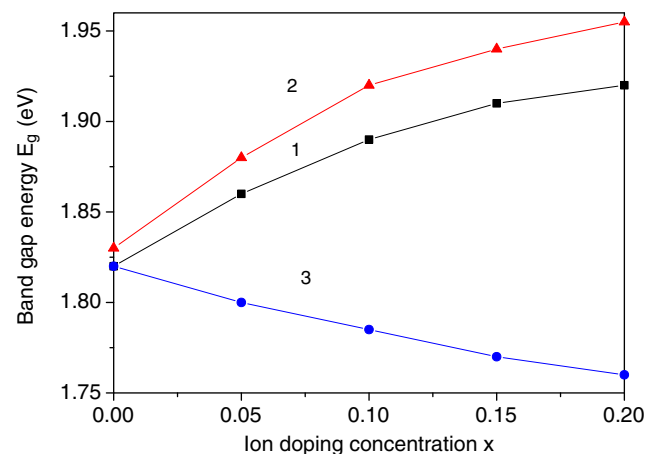


Figure 6. Ion doping concentration dependence of the bandgap energy E_g of a BFO NP ($N = 20$ shells) by Ni doping (1) with different $s-d$ interaction constants I : (1) $I = 0.5$ eV; (2) $I = 0.8$ eV. Note that in (3) x means the Zr doping concentration, $I = 0.5$ eV.

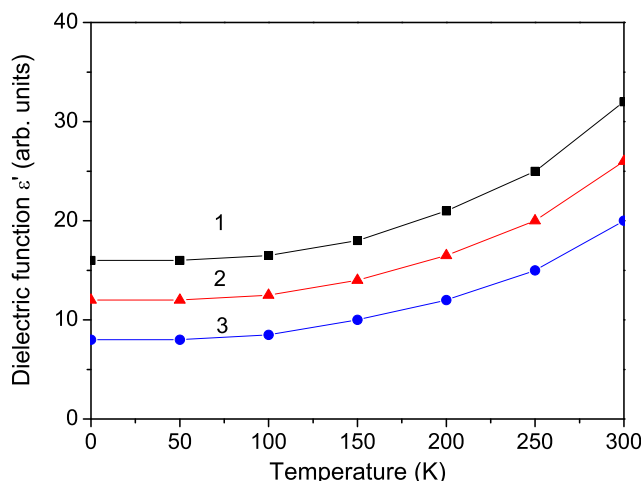


Figure 7. Temperature dependence of the dielectric function ϵ' of a pure BFO NP ($N = 20$ shells) for different magnetic fields h : (1) $h = 0$, (2) $h = 5$ kOe, (3) $h = 10$ kOe.

$J_d > J_b, J'_d < J'_b$.^[32] Further we have calculated the dielectric constant for Sm doping at the Fe and Ba sites. The results are shown also in Figure 5; the dielectric constant ϵ' increases for Sm substituting the Fe sites, whereas in the other case, the Ba sites, ϵ' decreases (see Figure 5). Note that we observe the opposite behavior for the magnetization: M_s decreases by Sm doping at the Fe sites and increases when Sm substitutes a Ba ion. We find a similar result for Sc^{3+} (0.88 Å) doping.

Finally, we demonstrate the magnetodielectric effect by evaluating the real part of the dielectric function ϵ' as a function of the external magnetic field h in the BFO NP at room temperature. The result is shown in Figure 7. The dielectric function ϵ' decreases with increasing field h as an indication for a negative magnetodielectric effect. A similar behavior is observed in pure, Sc-doped, and Co–Ti-codoped BFO NP.^[39,94,95] We argue that the effect is due to the change of the electric polarization induced by the magnetic field, i.e., to the magnetoelectric effect.^[95]

4. Conclusion

The main goal of our study is to demonstrate that the broad variety of properties of pure and doped BFO can be analyzed within a microscopic model where all relevant interactions are included, in particular the magnetocrystalline anisotropy K_1 in the magnetic subsystem. The Green's function technique allows us to find the magnetization expressed by the underlying spin wave excitations. The magnetization M_s is calculated for Ni, Zr, and Sm-doped BFO—bulk and nanoparticles. The size of the dopants expressed by the ionic radii is decisive for the evaluated macroscopic properties such as magnetization and polarization. Doping by Ni ions leads to a compressive strain, while doping with Zr gives rise to tensile strain. As a consequence, the microscopic interaction parameters such as exchange coupling, are changed accordingly. So the magnetization decreases with increasing Zr concentration due to the appearance of tensile strain, whereas M_s increases after Ni ion doping, which causes

a compressive strain. M_s increases whereas the coercive field H_c decreases with increasing particle size. Our microscopic model includes also an $s - d$ coupling between localized and itinerant spins. The related bandgap energy E_g was also evaluated. It can increase or decrease with increasing Ni or Zr doping concentration, which is related to quantum confinement effects. The $s - d$ shows a direct influence on the bandgap: E_g increases with the enhancement of the $s - d$ interaction strength.

The ferroelectric properties are characterized by the spontaneous polarization P_s and the real part of the dielectric constant ϵ' . These quantities can be computed likewise within our microscopic model. The polarization P_s and ϵ' increase with increasing Zr dopants, whereas they decrease due to Ni doping. The reason for the opposite behavior can be again traced back to the occurrence of the different kinds of strain originated by the dopants. The underlying magnetodielectric effect for the pure BFO NP is revealed in the decrease of the dielectric constant ϵ' with increasing magnetic field h .

The dielectric function ϵ' was calculated for rare earth ion doping at different sites. As a result, we found that ϵ' increases for Sm substitution at the Fe sites, whereas ϵ' decreases for substitution at the Ba sites. The magnetization M_s offers in these cases the opposite behavior.

All in all, the microscopic model and the related Green's function analysis allows a broad characterization of multiferroic properties by doping with other ions. The numerical evaluation of our analytical findings is in reasonable and good qualitative agreement with the experimental data.

Acknowledgements

A.T.A. acknowledges financial support by the Bulgarian National Fund "Scientific Studies" (contract no. KP-06-OPR 03/9).

Open access funding enabled and organized by Projekt DEAL.

Conflict of Interest

The authors declare no conflict of interest.

Data Availability Statement

The data that support the findings of this study are available from the corresponding author upon reasonable request.

Keywords

BaFe₁₂O₁₉ nanoparticles, bandgap, dielectric constant, ion-doped BaFe₁₂O₁₉, magnetization, polarization

Received: February 20, 2021

Revised: March 18, 2021

Published online: May 4, 2021

[1] R. C. Pullar, *Prog. Mater. Sci.* **2012**, *57*, 1191.

[2] U. Oezguer, Y. Alivov, H. Morkoc, *J. Mater. Sci.: Mater. Electron.* **2009**, *20*, 789.

- [3] V. P. Singh, R. Jasrotia, R. Kumar, P. Raizada, S. Thakur, K. M. Batoo, M. Singh, *World J. Condens. Matter Phys.* **2018**, *8*, 36.
- [4] G.-L. Tan, X. Chen, *J. Magn. Magn. Mater.* **2013**, *327*, 87.
- [5] M. G. Shalini, A. Subha, B. Sahu, S. C. Sahoo, *J. Mater. Sci.: Mater. Electron.* **2019**, *30*, 13647.
- [6] S. Che, J. Wang, Q. Chen, *J. Phys.: Condens. Matter* **2003**, *15*, L335.
- [7] J. K. Murthy, C. Mitra, S. Ram, A. Venimadhav, *J. Alloys Compd.* **2012**, *545*, 225.
- [8] J. Yu, S. Tang, L. Zhai, Y. Shi, Y. Dua, *Physica B* **2009**, *404*, 4253.
- [9] V. A. Zhuravlev, V. I. Itin, R. V. Minin, Y. M. Lopushnyak, D. A. Velikanov, *Russ. Phys. J.* **2018**, *60*, 1946.
- [10] V. Sepelak, M. Myndyk, R. Witte, J. Roder, D. Menzel, R. H. Schuster, H. Hahn, P. Heitjans, K.-D. Becker, *Faraday Discuss.* **2014**, *170*, 121.
- [11] X. Zhang, S. Meng, D. Song, Y. Zhang, Z. Yue, V. G. Harris, *Sci. Rep.* **2017**, *7*, 44193.
- [12] Y. Shao, F. Huang, X. Xu, S. Yan, C. Yang, M. Zhou, X. Lu, J. Zhu, *Appl. Phys. Lett.* **2019**, *114*, 242902.
- [13] G. Feng, W. Zhou, H. Deng, D. Chen, Y. Qing, C. Wang, F. Luo, D. Zhu, Z. Huang, Y. Zhou, *Ceram. Int.* **2019**, *45*, 13859.
- [14] L. Deng, Y. Zhao, Z. Xie, Z. Liu, C. Tao, R. Deng, *RSC Adv.* **2018**, *8*, 42009.
- [15] P. Behera, S. Ravi, *J. Supercond. Nov. Magn.* **2017**, *30*, 1453.
- [16] C. Liu, Y. Zhang, J. Jia, Q. Sui, N. Ma, P. Du, *Sci. Rep.* **2015**, *5*, 9498.
- [17] N. Dawar, M. Chitkara, I. S. Sandhu, J. S. Jolly, S. Malhotra, *Cogent Phys.* **2016**, *3*, 1208450.
- [18] G. Packiaraj, M. Hashim, K. C. B. Naidu, G. H. R. Joice, J. L. Naik, D. Ravinder, B. R. Rao, *Bioint. Res. Appl. Chem.* **2020**, *10*, 5455.
- [19] S. Vadivelan, N. V. Jaya, *Results Phys.* **2016**, *6*, 843.
- [20] V. N. Dhage, M. L. Mane, A. P. Keche, C. T. Birajdar, K. M. Jadhav, *Phys. B* **2011**, *406*, 789.
- [21] D. Chen, Y. Liu, Y. Li, K. Yang, H. Zhang, *J. Magn. Magn. Mater.* **2013**, *337–338*, 65.
- [22] G. Feng, W. Zhou, H. Deng, M. Yang, Y. Qing, F. Luo, D. Zhu, Z. Huang, Y. Zhou, C. Wang, *J. Mater. Sci.: Mater. Electron.* **2019**, *30*, 12382.
- [23] N. Tran, D. H. Kim, B. W. Lee, *J. Korean Phys. Soc.* **2018**, *72*, 731.
- [24] V. C. Chavan, S. E. Shirsath, M. L. Mane, R. H. Kadam, S. S. More, *J. Magn. Magn. Mater.* **2016**, *398*, 32.
- [25] A. Kumar, M. K. Verma, S. Singh, T. Das, L. Sibnh, K. D. Mandal, *J. Electron. Mater.* **2020**, *49*, 6436.
- [26] V. P. Singh, G. Kumar, A. Kumar, R. S. Rai, M. A. Valente, K. M. Batoo, R. K. Kotnala, M. Singh, *Ceram. Int.* **2014**, *42*, 5011.
- [27] S. Ounnunkad, *Solid State Commun.* **2006**, *138*, 472.
- [28] C. Wu, Z. Yu, K. Sun, J. Nie, R. Guo, H. Liu, X. Jiang, Z. Lan, *Sci. Rep.* **2016**, *6*, 36200.
- [29] C.-J. Li, B. Wang, J.-N. Wang, *J. Magn. Magn. Mater.* **2012**, *324*, 1305.
- [30] A. V. Trukhanov, K. A. Astapovich, M. A. Almessiere, V. A. Turchenko, E. L. Trukhanova, V. V. Korovushkin, A. A. Amirov, M. A. Darwish, D. V. Karpinsky, D. A. Vinnik, D. S. Klygach, M. G. Vakhitov, M. V. Zdorovets, A. L. Kozlovskiy, S. V. Trukhanov, *J. Alloys Compd.* **2020**, *822*, 153575.
- [31] X. Meng, Y. Ji, *J. Sol-Gel Sci. Technol.* **2013**, *67*, 18.
- [32] L. Wang, J. Zhang, Q. Zhang, N. Xu, J. Song, *J. Magn. Magn. Mater.* **2015**, *377*, 362.
- [33] G. M. Rai, M. A. Iqbal, K. T. Kubra, *J. Alloys Compd.* **2010**, *495*, 229.
- [34] P. Kumar, A. Gaur, *Ceram. Int.* **2017**, *43*, 16403.
- [35] G.-L. Tan, W. Li, *J. Am. Ceram. Soc.* **2015**, *98*, 1812.
- [36] P. S. Wang, H. J. Xiang, *Phys. Rev. X* **2014**, *4*, 011035.
- [37] V. Turchenko, A. Trukhanov, S. Trukhanov, M. Balasoiiu, N. Lupu, *J. Magn. Magn. Mater.* **2019**, *477*, 9.
- [38] V. A. Turchenko, A. M. Balagurov, S. V. Trukhanov, A. V. Trukhanov, *J. Synch. Invest.* **2019**, *13*, 69.
- [39] S. Gupta, S. K. Upadhyay, V. Siruguri, V. G. Sathe, E. V. Sampathkumaran, *J. Phys.: Condens. Matter* **2019**, *31*, 295701.
- [40] P. Sharma, A. Kumar, A. Dube, Q. Li, D. Varshney *AIP Conf. Proc.* **2016**, *1731*, 140010.
- [41] S. Ram, *J. Magn. Magn. Mater.* **1989**, *80*, 241.
- [42] A. Kumar, V. Agarwala, D. Singh, *Adv. Mater. Res.* **2012**, *585*, 62.
- [43] A. Kumar, V. Agarwala, D. Singh, *Prog. Electromagn. Res. M* **2013**, *29*, 223.
- [44] S. Agrawal, A. Parveen, A. Azam *AIP Conf. Proc.* **2016**, *1728*, 020205.
- [45] K. Habanjar, H. Shehabi, A. M. Abdallah, R. Awad, *Appl. Phys. A* **2020**, *126*, 402.
- [46] A. Banuelos-Frias, G. Martinez-Guajardo, L. Alvarado-Perea, L. Canizalez-Davalos, F. Ruiz, C. Valero-Lun, *Mater. Lett.* **2019**, *252*, 239.
- [47] X. Xu, W. Song, *Mater. Technol.* **2020**, *35*, 395.
- [48] J. Wang, F. Zhao, W. Wu, G.-M. Zhao, *J. Appl. Phys.* **2011**, *110*, 096107.
- [49] M. Okube, J. Yoshizaki, T. Toyodab, S. Sasakia, *J. Appl. Crystallogr.* **2016**, *49*, 1433.
- [50] S. V. Vonsovskij, *Magnetism*, John Wiley & Sons, New York, NY **1974**.
- [51] E. L. Nagaev, *Phys. Rep.* **2001**, *346*, 387.
- [52] J. Gutierrez, A. Lasheras, J. M. Barandiaran, R. Goncalves, P. Martins, S. Lanceros-Mendez, *IEEE Trans. Magn.* **2015**, *51*, 1.
- [53] V. G. Vaks, *Introduction to the Microscopic Theory of Ferroelectrics*, Nauka, Moscow **1973**, p. 158 (in Russian).
- [54] A. Isalgue, A. Labarta, J. Tejada, X. Obradors, *Appl. Phys. A* **1986**, *39*, 221.
- [55] N. Fuchikami, *J. Phys. Soc. Jpn.* **1965**, *20*, 760.
- [56] S. N. Zinenko, A. A. Murakhovski, L. P. Olkhovik, Z. I. Sizova, E. V. Shurinova, A. S. Kamzin, *J. Exp. Theor. Phys.* **2003**, *96*, 945.
- [57] R. A. McCurrie, S. Jackson, *J. Appl. Phys.* **1987**, *2*, 62.
- [58] H. Belrhazi, M. Y. El Hafidi, M. El Hafidi, *Res. Dev. Mater. Sci.* **2019**, *11*, 1143.
- [59] Z. V. Golubenko, L. P. Olkhovik, Yu. A. Popkov, Z. I. Sizova, A. S. Kamzin, *Phys. Solid State* **1998**, *40*, 1718.
- [60] M. V. Mamonova, *Phys. Solid State* **2020**, *62*, 777.
- [61] Z. W. Li, A. H. Morrish, *Phys. Rev. B* **1997**, *55*, 3670.
- [62] B. T. Shirk, W. R. Buessem, *J. Appl. Phys.* **1969**, *40*, 1294.
- [63] Z. Vakil, A. Kumar, A. Jain, K. M. Gupta, M. Najim and D. Singh, in *IEEE Int. Conf. Electrical, Computer and Communication Technologies (ICECCT)*, Coimbatore, India **2015**, pp. 1–4.
- [64] V. P. Singh, G. Kumar, A. Kumar, R. S. Raib, M. A. Valente, K. M. Batoo, R. K. Kotnala, M. Singh, *Ceram. Int.* **2016**, *42*, 5011.
- [65] X. Batlle, X. Obradors, M. Medarde, J. Rodriguez-Carvajal, M. Pernet, M. Vallet-Regi, *J. Magn. Magn. Mater.* **1993**, *124*, 228.
- [66] Y. Li, Q. Wang, H. Yang, *Current Appl. Phys.* **2009**, *9*, 1375.
- [67] A. S. Kumar, A. K. Bhatnagar, *AIP Conf. Proc.* **2018**, *1953*, 120068.
- [68] K. Yasui, K. Kato, *J. Phys. Chem. C* **2013**, *117*, 19632.
- [69] M. Glinchuk, A. Morozovskaya, *Phys. Status Solidi B* **2003**, *238*, 81.
- [70] S. Tjablikov, *Methods in the Quantum Theory of Magnetism*, Plenum Press, New York **1967**.
- [71] R. K. Mudsainiyan, S. K. Chawla, S. S. Meena, *J. Alloys Compd.* **2014**, *615*, 875.
- [72] M. N. Ashiq, R. B. Qureshi, M. A. Malana, M. F. Ehsan, *J. Alloys Compd.* **2014**, *617*, 437.
- [73] H. M. Khan, M. U. Islam, Y. Xu, M. A. Iqbal, I. Ali, *J. Alloys Compd.* **2014**, *589*, 258.
- [74] H. R. Zhai, J. Z. Liu, M. Lu, *J. Appl. Phys.* **1981**, *52*, 2323.
- [75] R. Guo, H. Li, P. Sun, Y. Li, Z. Zhao, M. Liu, *J. Cent. South Univ. Technol.* **2001**, *8*, 130.
- [76] D. Shekhawat, S. Verma, P. Sharma, *Trans. Indian Ceram. Soc.* **2017**, *76*, 247.
- [77] A. R. Al Dairy, L. A. Al-Hmoud, H. A. Khatatbeh, *Symmetry* **2019**, *11*, 732.
- [78] I. Bsoul, S. H. Mahmood, *J. Alloys Compd.* **2010**, *489*, 110.

- [79] A. V. Trukhanov, V. G. Kostishyn, L. V. Panina, S. H. Jabarov, V. V. Korovushkin, S. V. Trukhanov, E. L. Trukhanova, *Ceram. Int.* **2017**, *43*, 12822.
- [80] S. V. Trukhanov, A. V. Trukhanov, V. A. Turchenko, D. I. Tishkevich, E. L. Trukhanova, T. I. Zubar, D. V. Karpinsky, V. G. Kostishyn, L. V. Panina, D. A. Vinnik, S. A. Gudkova, E. A. Trofimov, P. Thakur, A. Thakur, Y. Yang, *J. Magn. Magn. Mater.* **2018**, *457*, 83.
- [81] K. Tanwar, D. S. Gyan, P. Gupta, S. Pandey, O. Parkash, D. Kumar, *RSC Adv.* **2018**, *8*, 19600.
- [82] M. F. Din, I. Ahmad, M. Ahmad, M. T. Farid, M. A. Iqbal, G. Murtaza, M. N. Akhtar, I. Shakir, M. F. Warsi, M. A. Khan, *J. Alloys Compd.* **2014**, *584*, 646.
- [83] A. Baykal, I. A. Auwal, S. Guener, H. Sozeri, *J. Magn. Magn. Mater.* **2016**, *430*, 29.
- [84] M. Wang, Q. Xu, S. Wang, Z. Wang, N. Ma, P. Du, *J. Alloys Compd.* **2018**, *765*, 951.
- [85] M. Waqar, M. A. Rafiq, T. A. Mirza, F. A. Khalid, A. Khaliq, M. S. Anwar, M. Saleem, *Appl. Phys. A* **2018**, *124*, 286.
- [86] R. R. Bhosale, R. S. Barkule, D. R. Shengule, K. M. Jadhav, *J. Mater. Sci.: Mater. Electron.* **2013**, *24*, 3101.
- [87] S. V. Trukhanov, A. V. Trukhanov, V. A. Turchenko, V. G. Kostishin, L. V. Panina, I. S. Kazakevich, A. M. Balagurov, *J. Magn. Magn. Mater.* **2016**, *417*, 130.
- [88] M. A. Almessiere, B. Unal, Y. Slimani, A. D. Korkmaz, N. A. Algarou, A. Baykal, *Results Phys.* **2019**, *14*, 102468.
- [89] B. C. Brightlin, S. Balamurugan, *J. Supercond. Nov. Magn.* **2017**, *30*, 215.
- [90] M. S. Rafique, S. Anjuma, K. Siraj, *Thin Solid Films* **2013**, *545*, 608.
- [91] J. Luo, Y. Xu, H. Mao, *J. Magn. Magn. Mater.* **2015**, *381*, 365.
- [92] N. Parween, PhD Thesis, National Institute of Technology, Kurukshetra **2014**.
- [93] R. B. Bylisma, W. M. Becker, J. Kossut, U. Debska, D. Yoder-Short, *Phys. Rev. B* **1986**, *33*, 8207.
- [94] X. Xu, F. Huang, Y. Shao, M. Zho, X. Ren, X. Lu, J. Zhu, *Phys. Chem. Chem. Phys.* **2017**, *19*, 18023.
- [95] Y. Guan, Y. Lin, L. Zou, Q. Miao, M. Zeng, Z. Liu, X. Gao, J. Liu, *AIP Adv.* **2013**, *3*, 122115.